

Atmospheric Chemistry
How to cite: *Angew. Chem. Int. Ed.* **2021**, *60*, 20200–20203

International Edition: doi.org/10.1002/anie.202105416

German Edition: doi.org/10.1002/ange.202105416

Mechanistic Study of the Aqueous Reaction of Organic Peroxides with HSO_3^- on the Surface of a Water Droplet

Hao Li⁺, Xiao Wang⁺, Jie Zhong, Biwu Chu, Qingxin Ma, Xiao Cheng Zeng,*
Joseph S. Francisco,* and Hong He*

Abstract: Aqueous reactions between organic peroxides and SO_2 are of intense interest in atmospheric science because of their ubiquitous implications for sulfate formation in secondary aerosols. However, the relative yields of the reaction products (inorganic vs. organic sulfates) remain controversial (i.e., 90% vs. 40–70% for inorganic sulfate) due in part to the lack of understanding of the underlying reaction mechanisms. Here, our computational results suggest that the reactions of HSO_3^- (dissolved SO_2) with organic peroxides are initiated on the surface of water nanodroplets and then proceed under two reaction pathways, in which the S atom of HSO_3^- attacks either the O1 or O2 atom of the peroxide group $-\text{O}(\text{O}2)\text{O}(\text{O}1)\text{H}$, leading to the formation of inorganic and organic sulfates, respectively. Notably, we find that the reaction initiated by O1 atom exhibits a relatively low energy barrier and high reaction rate, which favours the formation of inorganic sulfate.

Secondary organic aerosols (SOAs) account for a high percentage of tropospheric aerosols and thus exert significant impacts on the air quality, climate change, and human

health.^[1] As one of the major components in SOAs,^[2] organic peroxides are largely produced via the oxidation of volatile organic compounds (VOCs).^[3] For example, photooxidation of isoprene under low- NO_x conditions^[4] may produce organic peroxides accounting for $\approx 61\%$ of the SOA mass. Despite their prominent roles and major contributions to atmospheric SOAs, the underlying reaction mechanisms associated with the formation of inorganic/organic sulfates and their atmospheric fate in aerosols remain partially understood.^[5]

Recently, the reactions between organic peroxides and sulfur dioxide (SO_2) have attracted considerable attention, as the reaction products of inorganic and organic sulfates are accepted to be the major constituents of airborne fine particulate matter ($\text{PM}_{2.5}$) in the atmosphere.^[6] Wang et al.^[6b] found that the reactions between organic peroxide and SO_2 directly form organic sulfate, with the yield reaching as high as 60%, notably higher than that of inorganic sulfate. However, the experimental studies by Dovrou et al.^[6a] and Yao et al.^[6c] indicated relatively higher yields of inorganic sulfate, while the organic sulfate yields only reached 33%, 17% and 15% for the SO_2 reaction with isoprene hydroxyl hydroperoxide 1,2-ISOPOOH, 4,3-ISOPOOH, and α -pinene-derived peroxides, respectively. The apparent discrepancy in the relative yield of organic/inorganic products is attributed to multiple factors, including different reaction media, technical defects in product quantification, and distinct peroxide structures. Thus, to resolve the above discrepancy in the organic/inorganic yields between the different experiments, the actual reaction process must proceed with the same reaction medium and consistent techniques.

It should also be noted that none of the aforementioned experimental studies described the region (bulk vs. interface) in which aqueous reactions most likely occur. This information is crucial since bulk and interfacial water affect reaction pathways very differently. Specifically, the unique hydrogen-bond network formed at the air–water interface may enhance the adsorption and condensation of atmospheric species onto aerosols.^[7] Moreover, at the air–water interface, the activation barrier of aqueous reactions is lowered, thereby leading to different reaction pathways over those occurring in the bulk region.^[8] The aim of this computational study is to analyse whether reactions are most likely to occur at the surface or in the bulk region of water droplets, investigate the reaction pathways of aqueous reactions and compute the associated activation barriers to explore the reaction mechanisms underlying the aqueous reactions between organic peroxides and HSO_3^- . To this end, 1,2-ISOPOOH and $(\text{CH}_3)_3\text{COOH}$ (tert-butyl hydroperoxide) are selected as representative

[*] H. Li,^[†] Prof. B. W. Chu, Prof. Q. X. Ma, Prof. H. He
 State Key Joint Laboratory of Environment Simulation and Pollution Control, Research Center for Eco-environmental Sciences, Chinese Academy of Sciences
 Beijing, 100085 (China)
 E-mail: honghe@rcees.ac.cn



X. Wang^[†]
 School of Materials Science and Engineering, China University of Petroleum
 Qingdao, Shandong 266580 (China)

J. Zhong, Prof. J. S. Francisco
 Department of Earth and Environmental Science and Department of Chemistry, University of Pennsylvania
 Philadelphia, PA 19104-6316 (USA)
 E-mail: frjoseph@sas.upenn.edu

Prof. X. C. Zeng
 Department of Chemistry, University of Nebraska-Lincoln
 Lincoln, NE 68588 (USA)
 E-mail: xzeng1@unl.edu

Prof. B. W. Chu, Prof. Q. X. Ma, Prof. H. He
 Center for Excellence in Regional Atmospheric Environment, Institute of Urban Environment, Chinese Academy of Sciences
 Xiamen, 361021 (China)
 and
 University of Chinese Academy of Sciences
 Beijing, 100049 (China)

[†] These authors contributed equally to this work.

 Supporting information and the ORCID identification number(s) for the author(s) of this article can be found under:
 <https://doi.org/10.1002/anie.202105416>

organic peroxides, and the obtained results are compared to those reported in previous experiments.

In a previous study, HSO_3^- (produced from SO_2 in the aqueous phase) was shown to favour localization on the surface of a water droplet.^[9] Here, the surface preference of organic peroxides on water droplets is examined through classical molecular dynamics (MD) simulations (please refer to the Supporting Information for simulation details). Figure 1a depicts the time-dependent profile of the distances between the centre of mass of the chose peroxides (1,2-ISOPOOH) and that of the water droplet ($R_{\text{pero-droplet}}$). Initially, the 1,2-ISOPOOH molecule is placed inside the water droplet, and the corresponding $R_{\text{pero-droplet}}$ value is $\approx 1.18 \text{ \AA}$. With increasing MD simulation time, the $R_{\text{pero-droplet}}$ value gradually increases, indicating that 1,2-ISOPOOH moves towards the surface of the water droplet. At $\approx 150 \text{ ps}$, the diffusive motion of 1,2-ISOPOOH towards the air–water interface is completed as the $R_{\text{pero-droplet}}$ value is approximately the same as the radius of the water droplet. Thereafter, 1,2-ISOPOOH remains at the water surface. The surface preference of 1,2-ISOPOOH is also confirmed by the computed solvation free-energy profile vs. the radial direction of the water droplet (Figure 1b). As 1,2-ISOPOOH moves from vacuum to the interior region of the water droplet, the free-energy level attains a minimum at the air–water interface, after which it rises and eventually plateaus in the interior region of the droplet. In regard to $(\text{CH}_3)_3\text{COOH}$, a similar behaviour is observed, i.e., as it moves from vacuum to the surface of the water droplet at $\approx 125 \text{ ps}$ (as shown in Figure S1), the free-energy level also attains a minimum at the air–water interface. In sum, both ISOPOOH and

$(\text{CH}_3)_3\text{COOH}$ exhibit a surface preference when placed inside a water droplet.

Next, the reaction between 1,2-ISOPOOH or $(\text{CH}_3)_3\text{COOH}$ and HSO_3^- on the surface of a water droplet is investigated based on quantum chemistry calculations (details are provided in the Supporting Information). Here, we adopted a more realistic water nanodroplet system (consisting of 50 water molecules) instead of using the implicit solvation model typically adopted in mechanistic studies. Figures 2–5 show the optimized structures and

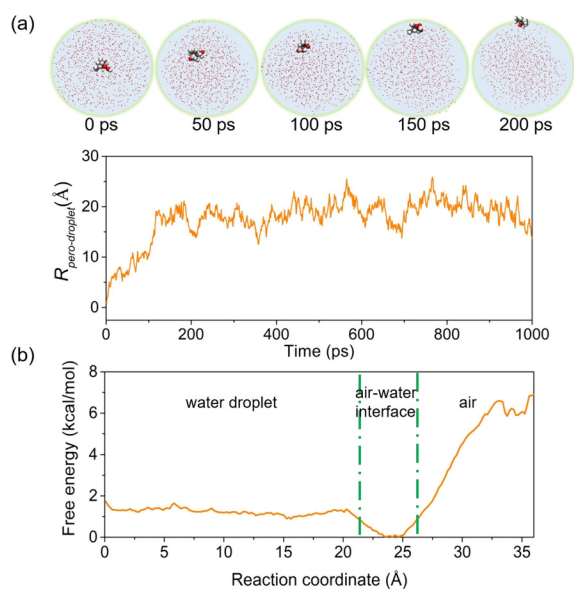


Figure 1. a) Snapshots of a 1,2-ISOPOOH molecule in a water nanodroplet vs. time and the time-dependent profile of the distance ($R_{\text{pero-droplet}}$, Å) between the centre of mass of the 1,2-ISOPOOH molecule and that of the water nanodroplet comprising 800 water molecules; b) solvation free-energy profile of 1,2-ISOPOOH as it moves from vacuum to the interior region of the water nanodroplet.

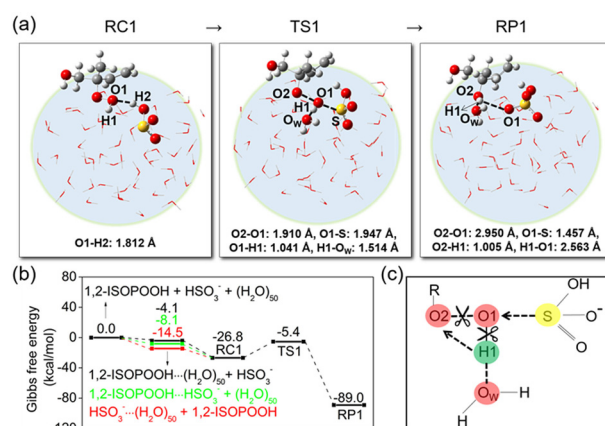


Figure 2. Reaction pathway towards the formation of *inorganic sulfate* via the reaction of 1,2-ISOPOOH and HSO_3^- at the surface of a water nanodroplet, based on the B3LYP-D3(BJ)/ma-def2-TZVPP//B3LYP-D3(BJ)/6-31+G** level of theory: a) Optimized structures of pre-reaction complex RC1, transition state TS1 and product RP1 [$\text{HOCH}_2\text{C}(\text{CH}_3)(\text{CH}=\text{CH}_2)(\text{OH})\cdots\text{HSO}_4^-\cdots(\text{H}_2\text{O})_{50}$], b) free-energy profile and c) a diagram of the reaction sites. Carbon, sulfur, oxygen and hydrogen atoms are represented by black, yellow, red and grey spheres, respectively.

energies of stationary points and the corresponding reaction pathway, where the transition-state (TS) structures are first searched by using B3LYP-D3(BJ) method with a 6-31+G** basis set. Once the TS structure is obtained, intrinsic reaction coordinate computation is adopted to confirm that the structure connects the desired reactants and products. Lastly, single-point energies are performed at the level of B3LYP-D3(BJ)/ma-def2-TZVPP method using the ORCA 4.2.0.^[10]

As shown in Figure 2, the reaction pathway indicates that reactions starting with the formation of the 1,2-ISOPOOH $\cdots\text{HSO}_3^-\cdots(\text{H}_2\text{O})_{50}$ (RC1) via three ways: (i) 1,2-ISOPOOH collides with adsorbed HSO_3^- on the water droplet; (ii) HSO_3^- collides with adsorbed 1,2-ISOPOOH on the water droplet; or (iii) the 1,2-ISOPOOH $\cdots\text{HSO}_3^-$ complex reacts on the water droplet. Here, the formation of 1,2-ISOPOOH $\cdots\text{HSO}_3^-\cdots(\text{H}_2\text{O})_{50}$ (RC1) is exothermic with an energy release of $-26.8 \text{ kcal mol}^{-1}$. From RC1, the reaction proceeds through the TS1, with an energy barrier of $21.4 \text{ kcal mol}^{-1}$ (with respect to RC1). Towards TS1, the S in HSO_3^- attacks the O1 in 1,2-ISOPOOH, while the H1 in 1,2-ISOPOOH attacks O_w in nearby interfacial water. Here, the interfacial water acts as a proton acceptor, assisting proton (H1) transfer from O1 to O2 of 1,2-ISOPOOH. Eventually,

$\text{HOCH}_2\text{C}(\text{CH}_3)(\text{CH}=\text{CH}_2)(\text{OH})\cdots\text{HSO}_3^- \cdots (\text{H}_2\text{O})_{50}$ (RP1) forms via atom transfer of O1 to S. The formed inorganic sulfate HSO_4^- is stable as the reaction product (RP1) reaches an extremely low energy level of $-89.0 \text{ kcal mol}^{-1}$. Additionally, based on the pseudo-steady-state approach (see details in Supporting Information), the liquid-phase rate constant for this reaction is evaluated as well, which is $1.30 \times 10^3 \text{ M}^{-1} \text{ s}^{-1}$ (Table S1), and its value is on the same order of magnitude as the measured rate constant.^[6a]

In addition to the formation of inorganic sulfate, the reaction of 1,2-ISOPOOH and HSO_3^- may yield organic sulfate through a distinct reaction mechanism (Figure 3). This

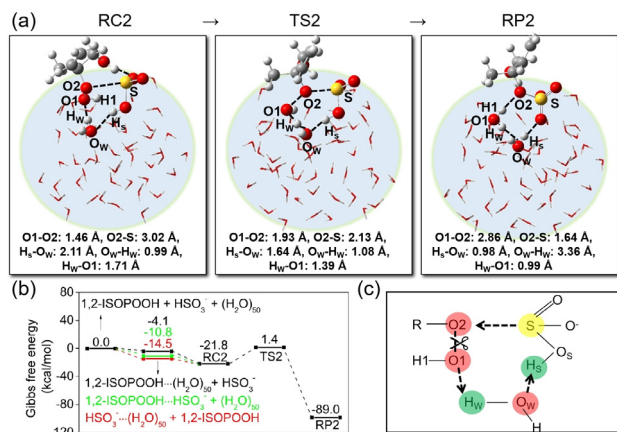


Figure 3. Reaction pathway towards the formation of *organic sulfate* via the reaction of 1,2-ISOPOOH and HSO_3^- at the surface of a water nanodroplet based on the B3LYP-D3(BJ)/ma-def2-TZVPP//B3LYP-D3-(BJ)/6-31+G** level of theory: a) Optimized structures of RC2, transition state TS2, and product RP2 [$\text{HOCH}_2\text{C}(\text{CH}_3)(\text{CH}=\text{CH}_2)(\text{OSO}_3^-) \cdots (\text{H}_2\text{O})_{51}$], b) free-energy profile and c) a diagram of the reaction sites. The atom colour codes are given in the caption of Figure 2.

reaction starts from the complex of 1,2-ISOPOOH $\cdots\text{HSO}_3^- \cdots (\text{H}_2\text{O})_{50}$ (RC2), which is located at an energy of $-21.8 \text{ kcal mol}^{-1}$. Thereafter, RC2 proceeds via TS2 and then forms a RP2 complex. In contrast to the formation mechanism of inorganic sulfate, organic sulfate formation is triggered by the S atom in HSO_3^- attacking O2 atom in 1,2-ISOPOOH and the breakage of O1 and O2 of 1,2-ISOPOOH, leading to the formation of organic sulfate, i.e., $\text{HOCH}_2\text{C}(\text{CH}_3)(\text{CH}=\text{CH}_2)(\text{OSO}_3^-)$. However, the relevant reaction rate constant is only $3.91 \times 10^{-1} \text{ M}^{-1} \text{ s}^{-1}$ (Table S1), much lower than that of inorganic sulfate formation ($1.30 \times 10^3 \text{ M}^{-1} \text{ s}^{-1}$), suggesting higher yield of inorganic sulfate than organic sulfate.

To examine whether the newly identified reaction mechanisms and relative yields of products are applicable to other organic peroxide, Figures 4 and 5 show the reaction pathway between $(\text{CH}_3)_3\text{COOH}$ and HSO_3^- . The reaction mechanisms of $(\text{CH}_3)_3\text{COOH}\cdots\text{HSO}_3^-$ are similar to those of 1,2-ISOPOOH $\cdots\text{HSO}_3^-$. Regarding the formation of inorganic sulfate (Figure 4), the O1 atom in $(\text{CH}_3)_3\text{COOH}$ is transferred to the S atom in HSO_3^- , and breakage of the O1-O2 bond occurs, while the H2 atom in HSO_3^- is transferred to the O2 atom with an interfacial water molecule functioning as the catalyst.

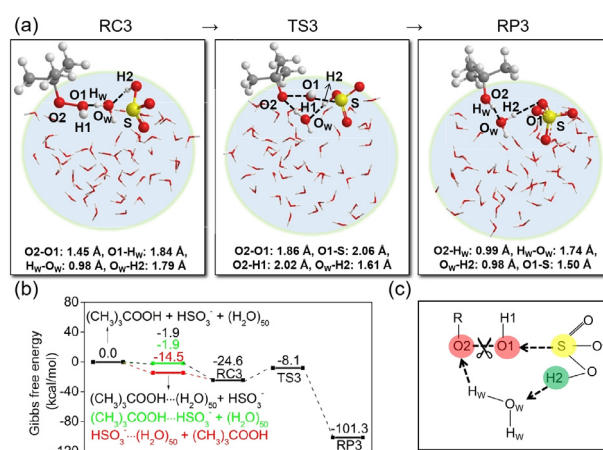


Figure 4. Reaction pathway towards the formation of *inorganic sulfate* via the reaction of $(\text{CH}_3)_3\text{COOH}$ and HSO_3^- at the surface of a water nanodroplet based on the B3LYP-D3(BJ)/ma-def2-TZVPP//B3LYP-D3-(BJ)/6-31+G** level of theory: a) optimized structures of RC3, transition state TS3, and product RP3 [$(\text{CH}_3)_3\text{C}(\text{OH})\cdots\text{HSO}_4^- \cdots (\text{H}_2\text{O})_{50}$], b) free-energy profile and c) a diagram of the reaction sites. The atom colour codes are given in the caption of Figure 2.

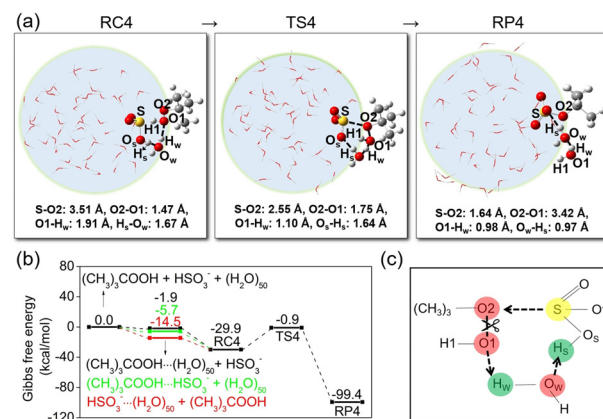


Figure 5. Reaction pathway towards the formation of *organic sulfate* via the reaction of $(\text{CH}_3)_3\text{COOH}$ and HSO_3^- at the surface of a water nanodroplet based on the B3LYP-D3(BJ)/ma-def2-TZVPP//B3LYP-D3-(BJ)/6-31+G** level of theory: a) optimized structures of RC4, transition state TS4, and product RP4 [$(\text{CH}_3)_3\text{C}(\text{OSO}_3^-) \cdots (\text{H}_2\text{O})_{51}$], b) free-energy profile and c) diagram of the reaction sites. The atom colour codes are given in the caption of Figure 2.

In regard to organic sulfate formation (Figure 5), the S atom in HSO_3^- is transferred to the O2 atom in $(\text{CH}_3)_3\text{COOH}$, while the O1-O2 bond breaks during the formation of the H_s-O1 bond. More importantly, the formation rate constant (see Table S1) of inorganic sulfate also exhibits a much higher value ($5.08 \times 10^6 \text{ M}^{-1} \text{ s}^{-1}$) than that of organic sulfate ($2.67 \times 10^1 \text{ M}^{-1} \text{ s}^{-1}$), again indicating a higher yield of inorganic sulfate.

In conclusion, both 1,2-ISOPOOH and $(\text{CH}_3)_3\text{COOH}$ tend to react with HSO_3^- to form both inorganic and organic sulfates, respectively, on the surface of a water nanodroplet [see reaction Equations (S1)–(S4)]. Both reactions are initiated via two distinct reaction pathways, i.e., the S atom in HSO_3^- attacks either the O1 or O2 atom in the peroxide

group -O(O₂)O(O₁)H. Considering that organic peroxides constitute an important atmospheric oxidation product and a ubiquitous component in various SOAs, the newly identified aqueous reactions between multiple organic peroxides and HSO₃⁻ are expected to occur widely in atmospheric environments, thereby contributing markedly to the formation of inorganic and organic sulfates in aerosols. These results suggest that heterogeneous water surface may play an important role in aerosol growth promotion via continued aqueous reactions. Overall, this study provides deeper mechanistic insights into the evolution of secondary inorganic and organic aerosols, and our findings may reconcile the discrepancy observed between previous experimental studies.

Acknowledgements

The research group of H. He was supported by the Chinese National Natural Science Foundation (22006158, 21922610, and 41877304), China Postdoctoral Science Foundation (2019M660818 and 2020TQ0339) and Special Research Assistant Project of the Chinese Academy of Sciences.

Conflict of Interest

The authors declare no conflict of interest.

Keywords: aqueous surface · HSO₃⁻ · organic peroxides · sulfates

- [1] a) R.-J. Huang, Y. Zhang, C. Bozzetti, K.-F. Ho, J.-J. Cao, Y. Han, K. R. Daellenbach, J. G. Slowik, S. M. Platt, F. Canonaco, P. Zotter, R. Wolf, S. M. Pieber, E. A. Brun, M. Crippa, G. Ciarelli, A. Piazzalunga, M. Schwikowski, G. Abbaszade, J. Schnelle-Kreis, R. Zimmermann, Z. An, S. Szidat, U. Baltensperger, I. El Haddad, A. S. H. Prevot, *Nature* **2014**, *514*, 218–222; b) Y. Sun, W. Du, P. Fu, Q. Wang, J. Li, X. Ge, Q. Zhang, C. Zhu, L. Ren, W. Xu, J. Zhao, T. Han, D. R. Worsnop, Z. Wang, *Atmos. Chem. Phys.* **2016**, *16*, 8309–8329.
- [2] a) B. Bonn, R. von Kuhlmann, M. G. Lawrence, *Geophys. Res. Lett.* **2004**, *31*, L10108; b) K. S. Docherty, W. Wu, Y. B. Lim, P. J. Ziemann, *Environ. Sci. Technol.* **2005**, *39*, 4049–4059.
- [3] a) M. H. Lee, B. G. Heikes, D. W. O'Sullivan, *Atmos. Environ.* **2000**, *34*, 3475–3494; b) R. Atkinson, J. Arey, *Chem. Rev.* **2003**, *103*, 4605–4638.
- [4] J. D. Surratt, S. M. Murphy, J. H. Kroll, N. L. Ng, L. Hildebrandt, A. Sorooshian, R. Szmigielski, R. Vermeylen, W. Maenhaut, M. Claeys, R. C. Flagan, J. H. Seinfeld, *J. Phys. Chem. A* **2006**, *110*, 9665–9690.
- [5] a) T. Liu, S. L. Clegg, J. P. D. Abbatt, *Proc. Natl. Acad. Sci. USA* **2020**, *117*, 1354–1359; b) J. Wang, J. Li, J. Ye, J. Zhao, Y. Wu, J. Hu, D. Liu, D. Nie, F. Shen, X. Huang, D. D. Huang, D. Ji, X. Sun, W. Xu, J. Guo, S. Song, Y. Qin, P. Liu, J. R. Turner, H. C. Lee, S. Hwang, H. Liao, S. T. Martin, Q. Zhang, M. Chen, Y. Sun, X. Ge, D. J. Jacob, *Nat. Commun.* **2020**, *11*, 2844; c) W. Wang, M. Liu, T. Wang, Y. Song, L. Zhou, J. Cao, J. Hu, G. Tang, Z. Chen, Z. Li, Z. Xu, C. Peng, C. Lian, Y. Chen, Y. Pan, Y. Zhang, Y. Sun, W. Li, T. Zhu, H. Tian, M. Ge, *Nat. Commun.* **2021**, *12*, 1993.
- [6] a) E. Dovrou, J. C. Rivera-Rios, K. H. Bates, F. N. Keutsch, *Environ. Sci. Technol.* **2019**, *53*, 12476–12484; b) S. Wang, S. Zhou, Y. Tao, W. G. Tsui, J. Ye, J. Z. Yu, J. G. Murphy, V. F. McNeill, J. P. D. Abbatt, A. W. H. Chan, *Environ. Sci. Technol.* **2019**, *53*, 10695–10704; c) M. Yao, Y. Zhao, M. Hu, D. Huang, Y. Wang, J. Z. Yu, N. Yan, *Environ. Sci. Technol. Lett.* **2019**, *6*, 768–774; d) E. Dovrou, K. H. Bates, J. C. Rivera-Rios, J. L. Cox, J. D. Shutter, F. N. Keutsch, *Atmos. Chem. Phys.* **2021**, *21*, 8999–9008; e) S. Wang, T. Liu, J. Jang, J. P. D. Abbatt, A. W. H. Chan, *Atmos. Chem. Phys.* **2021**, *21*, 6647–6661.
- [7] a) I. V. Stiopkin, C. Weeraman, P. A. Pieniazek, F. Y. Shalhout, J. L. Skinner, A. V. Benderskii, *Nature* **2011**, *474*, 192–195; b) M. D. Fayer, *Acc. Chem. Res.* **2012**, *45*, 3–14; c) J. Zhong, M. Kumar, C. Q. Zhu, J. S. Francisco, X. C. Zeng, *Angew. Chem. Int. Ed.* **2017**, *56*, 7740–7744; *Angew. Chem.* **2017**, *129*, 7848–7852; d) J. Zhong, M. Kumar, J. S. Francisco, X. C. Zeng, *Acc. Chem. Res.* **2018**, *51*, 1229–1237; e) J. Zhong, H. Li, M. Kumar, J. Liu, L. Liu, X. Zhang, X. C. Zeng, J. S. Francisco, *Angew. Chem. Int. Ed.* **2019**, *58*, 8351–8355; *Angew. Chem.* **2019**, *131*, 8439–8443; f) M. Galib, D. T. Limmer, *Science* **2021**, *371*, 921–925.
- [8] a) R. B. Gerber, M. E. Varner, A. D. Hammerich, S. Riikonen, G. Murdachaew, D. Shemesh, B. J. Finlayson-Pitts, *Acc. Chem. Res.* **2015**, *48*, 399–406; b) X. Yan, R. M. Bain, R. G. Cooks, *Angew. Chem. Int. Ed.* **2016**, *55*, 12960–12972; *Angew. Chem.* **2016**, *128*, 13152–13166; c) H. Wei, E. P. Vejerano, W. Leng, Q. Huang, M. R. Willner, L. C. Marr, P. J. Vikesland, *Proc. Natl. Acad. Sci. USA* **2018**, *115*, 7272–7277.
- [9] J. Yang, L. Li, S. Wang, H. Li, J. S. Francisco, X. C. Zeng, Y. Gao, *J. Am. Chem. Soc.* **2019**, *141*, 19312–19320.
- [10] F. Neese, *Wiley Interdiscip. Rev. Comput. Mol. Sci.* **2012**, *2*, 73–78.

Manuscript received: April 20, 2021

Accepted manuscript online: July 26, 2021

Version of record online: August 11, 2021